Protein-ligand binding affinity prediction: Is 3D binding pose needed?

Ming-Hsiu Wu **Ziqian Xie** **Degui Zhi** *
McWilliams School of Biomedical Informatics
University of Texas Health Science Center at Houston
Houston, TX, USA

Abstract

Accurate protein-ligand binding affinity prediction is crucial in drug discovery. Existing methods are predominately docking-free, without explicitly considering atom-level interaction between proteins and ligands in scenarios where crystallized protein-ligand binding conformations are unavailable. Now, with breakthroughs in deep learning AI-based protein folding and binding conformation prediction, can we improve binding affinity prediction? This study introduces a framework, Folding-Docking-Affinity (FDA), which folds proteins, determines protein-ligand binding conformations, and predicts binding affinities from three-dimensional protein-ligand binding structures. Our experiments demonstrate that the FDA outperforms state-of-the-art docking-free models in the DAVIS dataset, showcasing the potential of explicit modeling of three-dimensional binding conformations for enhancing binding affinity prediction accuracy.

1 Introduction

Protein-ligand binding affinity prediction is an important problem in drug discovery and computational biology. Accurately predicting the binding affinity between a protein and a small molecule ligand can help identify potential drug candidates and optimize drug design. Most existing binding affinity prediction methods leverage machine-learning methods, but they do not typically consider the binding pose, i.e., docking-free, hence ignoring the atom-level interactions between ligands and proteins, as shown in Fig 1(a). In these models, proteins are primarily represented as amino acid sequences or protein contact map graphs while SMILES strings or molecular graphs represent ligands. Deep neural networks are then applied to extract important latent features for predicting binding affinity (1; 2; 3; 4; 5; 6; 7; 8; 9). The classical models include DeepDTA (10), GraphDTA (11), DGraphDTA (12), and MGraphDTA (13). Additionally, for the sub-problem of kinase-drug binding affinity prediction, a specialized model, KDBNet, has also been proposed (14). It differs from the aforementioned models in that it incorporates features from predefined three-dimensional kinase binding pocket, thereby implicitly encodes the binding pose information. But this approach is specifically designed for the kinase-ligand binding affinity and may not be generalizable to wider-ranges of proteins. These docking-free methods often function as black-box models lacking structural context. Although they can be easily trained in an end-to-end manner, these docking-free methods may lack the interpretability and detailed insight into molecular interactions provided by docking approaches, potentially leading to less informed predictions.

Meanwhile, when co-crystallized 3D structures are available, there has been notable progress in the development of docking-based approaches, shown in Fig 1(b), that consider atom-level interactions explicitly (15; 16; 17; 18; 19; 20; 21; 22), exemplified by works like SchNet (23), EGNN (24), and GIGN (25). These works utilize 3D convolutional neural networks or interaction graph neural

*E-mail: Ming.Hsiu.Wu@uth.tmc.edu; Degui.Zhi@uth.tmc.edu

Preprint. Under review.

networks to predict binding affinity. Notably, these docking-based models could outperform their docking-free counterparts when testing on the PDBBind dataset (26) where a collection of high-resolution crystallized three-dimensional binding structures are curated. It is crucial to highlight, however, that this superiority would depend upon the availability of the three-dimensional binding structures. A pertinent question arises: in the absence of a high-resolution binding structure, can the docking-based model still maintain its advantage? This work aims to answer this question.

The premises of our question are the recent breakthroughs in deep learning-based protein folding and docking. Given AlphaFold (27; 28) and other methods (29; 30; 31; 32; 33; 34; 35) have revolutionized the field of protein folding, accessing three-dimensional protein structures become much easier than before. Simultaneously, deep learning-based protein-ligand docking models (36; 37; 38; 39) have been developed to generate binding conformations when provided with specific protein and ligand information much more easily, and their accuracy is catching up with computationally intensive molecular dynamics based docking. These advancements pave the way for a new approach to predict binding affinity in situations where a high-resolution crystal three-dimensional binding structure is not available.

Here, we present our framework, Folding-Docking-Affinity (FDA), illustrated in Fig 1(c), designed to fold proteins, determine optimal protein-ligand binding poses, and then predict binding affinity from computed three-dimensional binding structures. Notably, our approach is versatile and applicable to any protein-ligand pair. Here, we utilized ColabFold (31), a protein structure prediction model, DiffDock (36), a state-of-the-art deep learning-based docking model, and a GNN-based affinity predictor, GIGN (25), to build this framework. Importantly, any component of this framework can be substituted with alternative models. We expect that this approach enables reliable predictions of binding affinities of protein-ligand pairs without crystallized binding structures. Our assumption is that the docking-based method could outperform its docking-free counterparts by considering atom-level interactions, which more accurately reflect the true physical dynamics, even with minor deviation from the ground truth.

Our contributions are: We are the first to construct a general protein-ligand affinity prediction framework based on a computed explicit binding pose. We design the framework with individual replaceable components and thus can adapt to the fast-moving pace of folding, docking, and affinity prediction methods development. We demonstrated the feasibility of such methods by showing superior performance in a rigorous benchmark experiment in DAVIS (40). We quantify the noises introduced by the folding and docking steps in an ablation study.

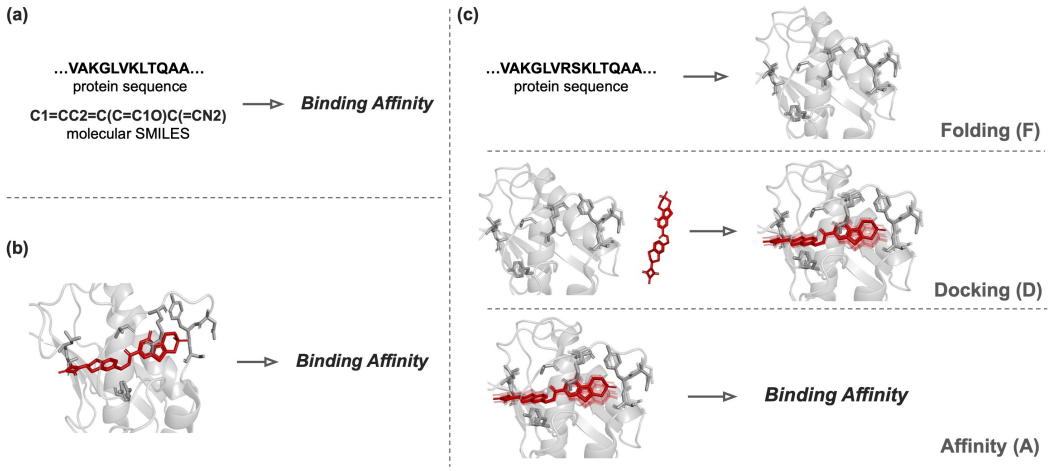

Figure 1: (a) Docking-free models predict binding affinity directly from a protein sequence and a molecular SMILES. (b) Docking-based models predict binding affinity directly from the experimentally determined crystallized binding structures. (c) Our work, Folding-Docking-Affinity (FDA), consists of three components: folding proteins (Folding), determining optimal protein-ligand binding poses (Docking), and predicting binding affinities from three-dimensional protein-ligand binding structures (Affinity).

2 Method

2.1 Framework

Our Folding-Docking-Affinity (FDA) framework consists of three components, shown in Fig 1(c): (i) Folding: Generating three-dimensional protein structures from protein amino acid sequences. (ii) Docking: Docking the ligand onto the generated protein structure. (iii) Affinity: Predicting binding affinities from predicted three-dimensional protein-ligand binding structure. Importantly, our framework features individual replaceable components, allowing it to adapt to various folding, docking, affinity prediction methods.

2.2 Models

We employed ColabFold (v1.5.5) (31) as our docking component to generate apo protein structures. The input comprises the MSA feature generated through MMseq2 (41) and template structures. The backend model architecture is Alphafold 2 multimer (v3)(28). We performed three prediction cycles for each structure and generated five structures for each protein. The top-ranked structure was subsequently relaxed using Amber, implemented in OpenMM (7.7.0) (42).

We utilized DiffDock (v1.0) (36), a score-based diffusion model, as the docking component. For each protein-ligand pair, we sampled ten binding poses. DiffDock comprises two parts: a diffusion generative model for ligand binding poses and a confidence score model. The former samples various binding poses by generating translational and rotational matrices, along with scalars representing the torsion angles of the ligand. Additionally, the confidence score model evaluates the quality of the binding pose sampled by the generative model. One key difference between the generative model and the confidence model is that the generative model only considers the alpha-carbon of the protein structure, whereas the confidence score model takes into account all heavy atoms of the protein. We directly used the pre-trained DiffDock models for the generation and subsequent ranking of the docking poses.

Furthermore, we incorporated the affinity predictor proposed by GIGN(25) to predict binding affinity based on the top-ranked generated binding poses. GIGN incorporates three essential components: the protein graph within the binding pocket area, the ligand graph, and the protein-ligand interaction graph. Additionally, during the graph message passing phase, the model treats covalent interactions and non-covalent interactions separately to enhance the effectiveness of learning node representations.

2.3 Dataset

We chose the DAVIS dataset to evaluate the effectiveness of our framework due to its consistency in measuring binding affinity (40) and its widespread use in benchmarking the performance of binding affinity predictors (10; 11; 12; 13). It's important to note that while the dataset provides binding affinity measurements, it lacks high-resolution crystallized binding structures. To our knowledge, this is the first study that employs three-dimensional protein-ligand binding conformations to analyze the DAVIS dataset. We adopted a similar method as in the KDBNet study (14) to select representative PDB structures of kinases. For kinases with several mutations in the Davis dataset, we retained only those with the minimal K_d values. The processed version includes 226 proteins, 64 ligands, and 14,464 binding affinity measurements. Additionally, we transformed the raw K_d values into pK_d values for model training. This transformation is defined as $pK_d = -\log_{10}(K_d/10^9)$, which aids in model convergence by ensuring numerical stability.

We also follow the KDBNet study to establish four train-test split settings to assess prediction performance: (1) new-protein split: 20% of kinases were held back as the test set, mimicking a drug repositioning scenario where the model makes predictions for unseen proteins. (2) New-drug split: 20% of drugs were set aside as the test set, emulating a drug discovery scenario where the model makes predictions for unseen drugs. (3) Both-new split: 20% of kinases and 20% of drugs were held out as the test set, representing a scenario where the model makes predictions for both unseen proteins and drugs. (4) Sequence-identity split: Similar to the new-protein split, but with the additional criterion that no kinase in the training set shares more than 50% sequence identity with any kinase in the test set.

Regarding the three-dimensional ligand structure, we directly download the ligand structure from PubChem database (43) based on the ligand's compound identifier (CID). For three-dimensional protein structures, we leveraged the ColabFold (31) to generate the three-dimensional protein structures from the corresponding amino acid sequences. Both three-dimensional protein and ligand structures were represented as heterogeneous geometric graphs. Our node and edge feature representations follow those used in DiffDock (36).

2.4 Ablation study

Due to the limited availability of crystallized binding structures for most protein-ligand pairs in the DAVIS dataset, we opted to use the PDBBind (version 2016) dataset (26) as our training and validation set. We excluded protein-ligand pairs where (i) the protein with amino acid sequence longer than 3000, due to time constraints for protein folding, (ii) DiffDock failed to dock the ligand onto the protein, and (iii) DiffDock-generated ligand could not be processed by RDKit (version 2022.9.5). Ultimately, the training set consists of 11,637 protein-ligand pairs, while the validation set comprises 975 pairs.

Additionally, we identified 102 protein-ligand pairs from the DAVIS dataset that have available three-dimensional crystallized PDB structures in the RCSB database (44). To create our test set for the ablation study, we excluded 49 pairs that were already present in the DiffDock training set, resulting in a final set of 53 pairs.

The protein generated by ColabFold relies on the amino acid sequence extracted from the FASTA file within the RCSB database (44). This sequence serves as ColabFold's input. Additionally, for the three-dimensional ligand structure, we employ the Tripos molecule structure format (MOL2), which is provided by PDBbind (26).

The initial step in calculating the Root Mean Square Error (RMSE) for the binding pocket involves aligning the apo ColabFold protein structure with the holo crystal protein structure. For the protein generated by ColabFold, we extracted the amino acid sequence from the FASTA file in the RCSB database (44). To reconcile discrepancies such as missing amino acids in the crystal PDB file, we employed Biopython (45) for global sequence alignment, identifying the shared subsequence between the FASTA and PDB file.

Next, we utilized alpha-carbon atoms for the structure alignment, following the methodology outlined in the DiffDock work (36). This approach utilizes the weighted Kabsch algorithm. For each alpha-carbon atom x, its weight is described as $w_x = e^{-\lambda d_x}$ where λ represents a smoothing factor, and d_x corresponds to the minimum distance of x to a ligand atom within the protein-ligand complex. In this way, the alpha-carbon atom that is closer to the ligand is assigned a higher weight. Details of λ selection can be found in the DiffDock work (36).

After aligning the two protein structures, we calculated the RMSE using all non-hydrogen atoms within a 5 Å radius from the ligands (46), except for residues where the apo ColabFold protein and the crystallized protein have different numbers of non-hydrogen atoms.

3 Result

3.1 Affinity prediction benchmark

Based on our experimental results, our FDA model generally outperforms the other docking-free models in four different split test sets shown in Fig. 2. In particular, our model demonstrates its exceptional performance in the most demanding task: the 'both-new' split. This split involves proteins and ligands in the test set that are not present in the training set, highlighting the generalizability of our model. It is noteworthy that while MGraphDTA performs well on the random split, as illustrated in Fig.S1, where proteins and ligands in the test set have some overlap with the training set, its performance significantly declines in the more challenging scenarios. This drop in the performance of the docking-free model indicates potential overfitting and low generalizability. The same trend was also observed in the prior research (25). These findings underscore the advantage of our approach, which explicitly accounts for the protein-ligand binding conformations, in enhancing model generalizability when compared to other docking-free methods. Moreover, within our FDA framework, the use of ColabFold-generated apo-structures, in comparison to crystallized holo-

structures —yielded a surprising improvement in affinity prediction performance. This enhancement was mostly observed in both Pearson correlation and Mean Squared Error (MSE) metrics, with the exception of the both-new split, as illustrated in Figure S2.

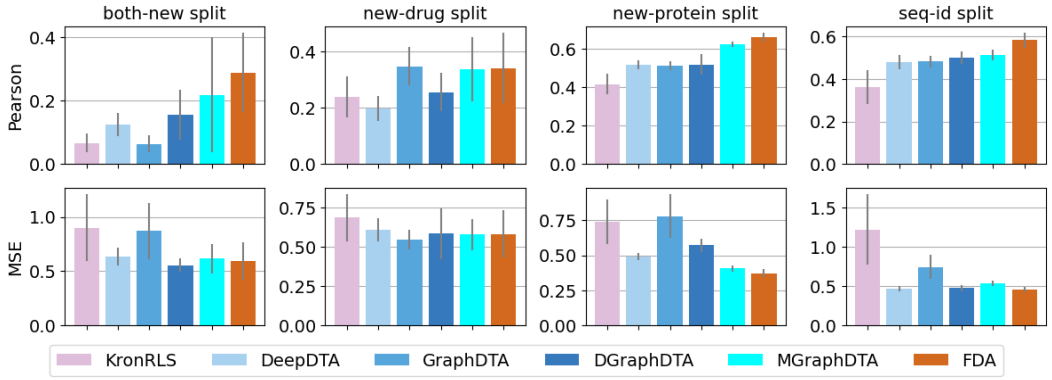

Figure 2: Comparison of FDA prediction performance with docking-free methods KronRLS, DeepDTA, GraphDTA, DGraphDTA, and MGraphDTA in four train-test split settings. Bar plots display the average $\pm$ standard deviation of the evaluation results across five randomly chosen train/test splits. Pearson correlation and Mean Squared Error (MSE) were calculated based on the predicted and true pK_d values. The experimental results of KronRLS, DeepDTA, GraphDTA, and DGraphDTA are extracted from (14).

3.2 Ablation study

In our affinity prediction benchmark using the DAVIS dataset, where we tested the FDA method alongside other docking-free methods, our FDA approach generally outperformed these methods. However, the impacts of the deviation introduced by ColabFold and DiffDock on the final affinity prediction remain unclear. To address this, we designed ablation experiments with three distinct scenarios: (i) Crystal binding poses (Crystal-Crystal): Protein-ligand binding structures are determined solely through experiments, with no deviation introduced by ColabFold and DiffDock. (ii) Holo Crystal Proteins with DiffDock (Crystal-DiffDock): In this scenario, we utilize holo Crystal Proteins for protein structures and employ DiffDock to determine the ligand binding pose. (iii) Apo ColabFold with DiffDock (ColabFold-DiffDock): In this case, we use apo ColabFold protein structures and again utilize DiffDock to find the ligand binding pose. Details of the experimental setting can be found in Method. Given the limited availability of crystallized binding structures for most protein-ligand pairs in the DAVIS dataset, we utilized the PDBBind (version 2016) dataset (26) with the three settings mentioned above to train three distinct affinity prediction models: Crystal-Crystal, Crystal-DiffDock, and ColabFold-DiffDock. After training, we assessed the performances of these models using a test set selected from the DAVIS dataset. This test set consists of protein-ligand pairs with crystallized binding structures so that we can similarly curate three test sets under our three settings.

The performance of three distinct models on various test sets is illustrated in Fig. 3. Initially, we hypothesize that the model trained using the Crystal-Crystal dataset could exhibit the best prediction performance on the Crystal-Crystal test set (indicated by the lightest color), while the ColabFold-DiffDock model predicting the ColabFold-DiffDock dataset could show the worst performance (represented by the darkest color). This assumption is based on the potential error introduced by ColabFold and DiffDock, which may impact the model's performance. On the contrary, our observations reveal that the lowest root mean square error (RMSE) is observed in the ColabFold-DiffDock model predicting the Crystal-Crystal dataset, while the highest Pearson correlation coefficient (R_p) is found in the Crystal-DiffDock model predicting the Crystal-Crystal dataset. Furthermore, the model trained on the ColabFold-DiffDock dataset generally performs better across three test sets than the other two scenarios, as shown in Fig. 3.

Table 1 presents the values corresponding to the diagonal line of Fig. 3. In other words, the table exclusively displays the performance of the three distinct prediction models evaluated on their corresponding datasets. Comparing the performance of ColabFold-DiffDock models with other SOTA

Table 1: The ablation experiment involved three distinct scenarios, each with its corresponding average (standard deviation) of root-mean-square error (RMSE) and average (standard deviation) Pearson correlation coefficient (R_p) for affinity prediction, tested ten times.

3D-based methods			
Folding	Docking	RMSE ↓	R_p ↑
Holo crystal protein	Crystal ligand pose	**1.42**(0.04)	**0.15**(0.07)
Holo crystal protein	DiffDock pose	1.49(0.04)	0.07(0.08)
Apo ColabFold protein	DiffDock pose	1.43(0.05)	0.12(0.07)
1D-based methods			
MGraphDTA		1.51(0.08)	0.09(0.11)
GraphDTA		1.76(0.10)	-0.04(0.09)

Table 2: The average (standard deviation) root-mean-square error (RMSE) in the unit of Å, of protein binding pocket and ligand binding poses introduced by ColabFold and DiffDock in the three distinct scenarios.

	PDBBind(2016) training set		DAVIS-53 test set	
	Folding (F)	Docking (D)	Folding (F)	Docking (D)
Crystal-Crystal	0	0	0	0
Crystal-DiffDock	0	5.27(22.54)	0	2.30(4.95)
ColabFold-DiffDock	1.30(1.24)	16.68(624.35)	1.27(0.40)	3.18(4.23)

docking-free methods, our framework generally achieves better on Pearson correlation (R_p) and root mean square error (RMSE).

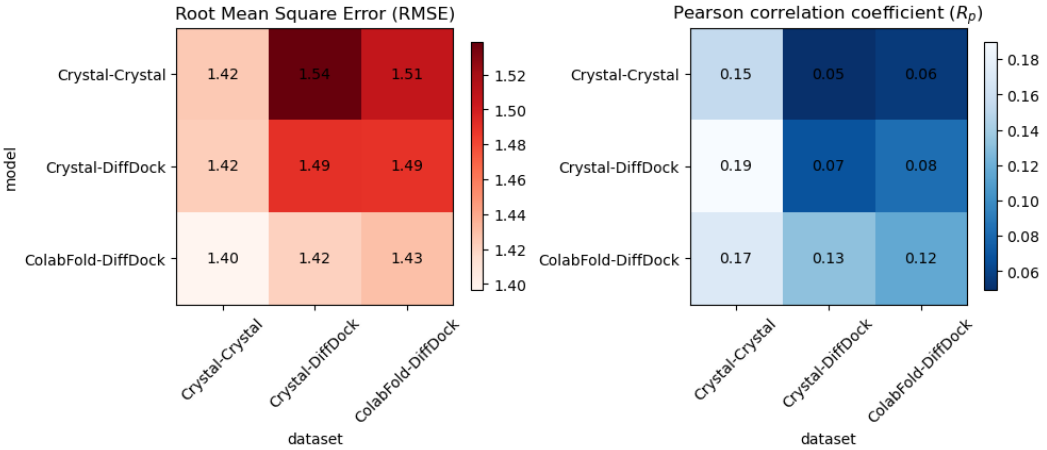

Figure 3: The heatmap displays the Root Mean Square Error (RMSE) and the Pearson correlation coefficients (R_p) for various prediction models across different test datasets in the ablation study.

In our ablation study, we tested three distinct scenarios within our FDA framework. To our surprise, the ColabFold-DiffDock combination generally achieved better performance. To better investigate these counter-intuitive results, we sought to quantify the deviation introduced by ColabFold and DiffDock. We calculated the RMSE of the ligand pose and the RMSE of the protein binding pocket structure. The results of these calculations are presented in Table 2. In the Crystal-Crystal combination, both the RMSE of the protein binding pocket structure and ligand poses are equal to zero. In the Crystal-DiffDock combination, only DiffDock is used to find the binding pocket and ligand binding pose, while the protein structures remain in their crystallized coordinates. Therefore, only the RMSE of the ligand binding poses is calculated. In the ColabFold-DiffDock combination, where both ColabFold and DiffDock are simultaneously utilized to generate binding conformations, both the RMSE of the protein binding pocket structures and ligand binding poses are calculated. When comparing the Crystal-DiffDock and ColabFold-DiffDock combinations, we observed that using DiffDock to dock ligands onto ColabFold-generated structures resulted in a higher average RMSE

and standard deviation of ligand binding poses compared to using crystallized protein structures. This trend aligns with the findings from DiffDock's work, where they tested their method on ESMfold-generated proteins (36). In the discussion section, further exploration of potential explanations for the counter-intuitive result will be presented.

4 Discussion and Conclusion

This study mainly answers the question of whether a docking-based model surpasses a docking-free model in predicting protein-ligand binding affinity when high-resolution binding structures are unavailable. Our experiments demonstrate that our FDA method surpasses the current leading docking-free method on four train-test split settings. Therefore, we propose that three-dimensional binding conformations are crucial for binding affinity prediction.

4.1 DAVIS dataset

DAVIS comprises 442 proteins, 68 ligands, and 30,056 binding affinity measurements (K_d) but without high-resolution binding structures. It is worth noting that the truncated K_d (K_d values are greater than 10 uM) make up the majority of the DAVIS dataset (around 70%), which leads to challenges in the model training. Meanwhile, we have identified proteins within the dataset that exhibits modifications, such as mutations and phosphorylations. Previous studies (10; 11; 13; 9) tend to overlook the impact of these modifications, treating modified and unmodified proteins as equivalent. We argue that such modifications could significantly influence binding affinity predictions, and including them indiscriminately is not a prudent approach to leverage the dataset. In the future, we will consider these mutations and construct the corresponding three-dimensional protein structures to curate a more comprehensive dataset.

Secondly, given that the DAVIS dataset only provides Uniprot IDs for protein information and lacks details on the protein binding site, selecting appropriate protein structures presents a challenge. In our current work, we chose to directly utilize pre-defined PDB structures, as in the work of KDBnet (14), to represent three-dimensional structures of kinases. However, it should be noted that only half of the kinases in DAVIS have defined PDB structure, resulting in the under-utilization of the remaining data. An alternative approach involves incorporating the entire amino acid sequence of a Uniprot ID to construct the corresponding three-dimensional protein structure, which can be obtained from the Alphafold database. However, this method significantly expands the search space of DiffDock and increases the complexity of identifying the correct binding pockets. As a result, the predictive accuracy of ligand binding poses decreases compared to using PDB structures, illustrated in Fig.S2. Therefore, we believe that constraining the protein search space is necessary in our FDA framework.

Despite its inherent challenges, it offers a valuable resource by including several protein targets with mutations and phosphorylation and their corresponding binding affinity. An interesting next step is to check if affinity predictors can discern the affinity difference between these modifications. Importantly, past studies have overlooked these changes, emphasizing the necessity of paying closer attention to the DAVIS dataset in future research. The dataset's inclusion of various modifications provides a chance to deepen our knowledge of protein-ligand interactions and improve predictive models to handle these variations.

4.2 The effect of noise

In our ablation study, the model trained on apo ColabFold proteins with DiffDock-generated poses, appears to be particularly interesting. Initially anticipated as potentially the worst performing model due to the introduction of noise by ColabFold and DiffDock as shown in Table. 2, surprisingly, it generally demonstrated better performance across all three test sets. We posit that through the addition of noise to binding conformations by ColabFold and DiffDock, these models seem to learn from a smoother affinity profile toward various binding conformations. This could be advantageous for the prediction of binding affinity in various situations.

Despite observing a consistent trend in both our benchmark study and ablation study, the potential underlying mechanism remains unclear, necessitating further investigation and experimental exploration. Our analysis suggests that the noise introduced into protein structure can be separated

into two distinct components: (i) The structural difference between the apo protein and the holo protein. (ii) The noise introduced by ColabFold in predicting the apo protein. Similarly, when examining the noise associated with the ligand, it can be broken down into two components: (i) Docking the ligand to apo protein instead of the holo protein. (ii) The intrinsic uncertainty of DiffDock.

In our future work, we plan to explore the structural differences between the apo protein and the holo protein. Additionally, we aim to manually introduce noise into the binding conformation by slightly perturbing the torsion angles of ligands and the torsion angles of the protein backbone and sidechains within the binding pocket area. Determining the optimal distribution of this introduced noise will be a focus of our future research.

Given that most PDB structures in the RCSB database (44) only include partial protein amino acid sequences, we conducted tests using the entire-sequence Alphafold-generated protein structures to assess performance differences. Surprisingly, we observed that this approach does not improve the performance; rather, it diminishes it, as shown in Fig.S2. Our analysis suggests that this method significantly broadens the search space of DiffDock, consequently amplifying the complexity of identifying the correct binding pockets. This leads to an introduction of excessive noise into the binding conformation. As a result, our primary aim is to investigate how adding noise strategically can optimally enhance the prediction of binding affinity. We aim to uncover the subtle ways in which noise can influence and potentially improve the accuracy of affinity predictions, thereby shedding light on the intricate dynamics of molecular interactions within the binding pocket in the context of deep learning.

4.3 KDBNet comparison

KDBNet (14) is a recent publication that similarly takes into account the three-dimensional structures of protein binding pockets and ligands to predict binding affinity. However, unlike our framework, it does not incorporate binding conformations. We compared our method with the KDBNet results and found that KDBNet outperforms our approach, as demonstrated in Fig.S3. It is important to note that KDBNet is specifically designed for kinases, which have well-identified and well-studied binding pockets. In contrast, our framework operates without the constraints of a predefined binding pocket, allowing us to explore binding interactions across various protein families.

The success of KDBNet highlights the potential benefits of incorporating feature-based model architectures. Inspired by this approach, we aim to explore the integration of similar elements into our future method development. This could involve leveraging pre-defined binding pockets when available, while retaining the flexibility to handle proteins lacking such well-defined regions. This combined approach has the potential to enhance prediction accuracy for specific targets while maintaining the current versatility for broader protein families.

4.4 Conclusion

In this study, we introduce a flexible framework, Folding-Docking-Affinity (FDA), for predicting protein-ligand binding affinity. This framework leverages explicitly computed binding poses, and features with interchangeable components, ensuring its adaptability to the rapidly evolving folding, docking, and affinity prediction methods. Our experiments demonstrate that our framework surpasses state-of-the-art docking-free models. This highlights the potential of using computed protein-ligand three-dimensional binding conformation to enhance the accuracy of the binding affinity prediction. Moreover, recent advancements in more innovative deep learning-based models, such as the updated versions of DiffDock, DiffDock-L (47), and DynamicBind (48), are noteworthy. DiffDock-L aims to improve generalizability across different types of proteins, while DynamicBind accounts for the flexibility of protein structures, which are often treated as rigid bodies in other deep learning methods. We are confident that these advancements in molecule docking will greatly enhance the performance of our proposed framework. Additionally, our exploration led to an unexpected discovery: the introduction of noise by ColabFold and DiffDock appears to have a beneficial impact on binding affinity prediction and generalizability across diverse datasets. This interesting finding suggests that the strategic incorporation of noise may hold promise for improving the robustness and performance of binding affinity predictors. We suggest that high-resolution binding conformations are not necessarily crucial for affinity prediction; Instead, introducing moderate noise could potentially

enhance the prediction performance. The success of the FDA framework underscores the importance of integrating multi-dimensional structural information into deep learning frameworks for enhanced predictive capabilities. Moving forward, we aim to delve deeper into the mechanisms underlying the impact of noise on model performance, as well as explore additional strategies to further refine our FDA approach. These advancements hold the potential for advancing the field of computational drug discovery and facilitating the design of novel therapeutics with improved efficacy and generalizability.

5 Data availability

The processed data can be accessed at https://zenodo.org/records/10968593. This dataset includes the ColabFold-generated apo protein structures and the DiffDock-generated ligand binding poses for the affinity prediction benchmark. Additionally, for the ablation study, the repository contains three-dimensional structures of protein-ligand complexes under three scenarios (Crystal-Crystal, Crystal-DiffDock, ColabFold-DiffDock).

6 Code availability

The source code of the FDA is available at our GitHub repository https://github.com/ZhiGroup/FDA

7 Author contributions

MH.W, Z.X, and D.Z conceived the research project. Z.X, and D.Z supervised the research project. MH.W developed the computational method, implemented the software, and performed the evaluation analyses. All authors analyzed the results and participated in the interpretation. MH.W wrote the manuscript with support from all other authors.

8 Competing interests

The authors declare no competing interests.

References

[1] Lee, I., Keum, J. & Nam, H. Deepconv-dti: Prediction of drug-target interactions via deep learning with convolution on protein sequences. *PLoS computational biology* **15**, e1007129 (2019).

[2] Abbasi, K. *et al.* Deepcda: deep cross-domain compound–protein affinity prediction through lstm and convolutional neural networks. *Bioinformatics* **36**, 4633–4642 (2020).

[3] Rifaioglu, A. S. *et al.* Mdeepred: novel multi-channel protein featurization for deep learning-based binding affinity prediction in drug discovery. *Bioinformatics* **37**, 693–704 (2021).

[4] Huang, L. *et al.* Coadti: multi-modal co-attention based framework for drug–target interaction annotation. *Briefings in Bioinformatics* **23**, bbac446 (2022).

[5] Yuan, W., Chen, G. & Chen, C. Y.-C. Fusiondta: attention-based feature polymerizer and knowledge distillation for drug-target binding affinity prediction. *Briefings in Bioinformatics* **23**, bbab506 (2022).

[6] Huang, K., Xiao, C., Glass, L. M. & Sun, J. Moltrans: molecular interaction transformer for drug–target interaction prediction. *Bioinformatics* **37**, 830–836 (2021).

[7] Zeng, Y., Chen, X., Luo, Y., Li, X. & Peng, D. Deep drug-target binding affinity prediction with multiple attention blocks. *Briefings in bioinformatics* **22**, bbab117 (2021).

[8] Wang, K., Zhou, R., Li, Y. & Li, M. Deepdtaf: a deep learning method to predict protein–ligand binding affinity. *Briefings in Bioinformatics* **22**, bbab072 (2021).

[9] Nguyen, T. M., Nguyen, T., Le, T. M. & Tran, T. Gefa: Early fusion approach in drug-target affinity prediction. *IEEE/ACM Transactions on Computational Biology and Bioinformatics* **19**, 718–728 (2022).

[10] Öztürk, H., Özgür, A. & Ozkirimli, E. Deepdta: Deep drug-target binding affinity prediction. *Bioinformatics* **34**, i821–i829 (2018).

[11] Nguyen, T. *et al.* Graphdta: predicting drug–target binding affinity with graph neural networks. *Bioinformatics* **37**, 1140–1147 (2021).

[12] Jiang, M. *et al.* Drug–target affinity prediction using graph neural network and contact maps. *RSC advances* **10**, 20701–20712 (2020).

[13] Yang, Z., Zhong, W., Zhao, L. & Chen, C. Y.-C. Mgraphdta: deep multiscale graph neural network for explainable drug–target binding affinity prediction. *Chemical science* **13**, 816–833 (2022).

[14] Luo, Y., Liu, Y. & Peng, J. Calibrated geometric deep learning improves kinase–drug binding predictions. *Nature Machine Intelligence* **5**, 1390–1401 (2023).

[15] Jiang, D. *et al.* Interactiongraphnet: A novel and efficient deep graph representation learning framework for accurate protein–ligand interaction predictions. *Journal of medicinal chemistry* **64**, 18209–18232 (2021).

[16] Sánchez-Cruz, N., Medina-Franco, J. L., Mestres, J. & Barril, X. Extended connectivity interaction features: improving binding affinity prediction through chemical description. *Bioinformatics* **37**, 1376–1382 (2021).

[17] Stepniewska-Dziubinska, M. M., Zielenkiewicz, P. & Siedlecki, P. Development and evaluation of a deep learning model for protein–ligand binding affinity prediction. *Bioinformatics* **34**, 3666–3674 (2018).

[18] Wang, Y., Wu, S., Duan, Y. & Huang, Y. A point cloud-based deep learning strategy for protein–ligand binding affinity prediction. *Briefings in Bioinformatics* **23**, bbab474 (2022).

[19] Zheng, L. *et al.* Improving protein–ligand docking and screening accuracies by incorporating a scoring function correction term. *Briefings in Bioinformatics* **23**, bbac051 (2022).

[20] Moon, S., Zhung, W., Yang, S., Lim, J. & Kim, W. Y. Pignet: a physics-informed deep learning model toward generalized drug–target interaction predictions. *Chemical Science* **13**, 3661–3673 (2022).

[21] Wang, Z. *et al.* Onionnet-2: a convolutional neural network model for predicting protein-ligand binding affinity based on residue-atom contacting shells. *Frontiers in chemistry* **9**, 753002 (2021).

[22] Jones, D. *et al.* Improved protein–ligand binding affinity prediction with structure-based deep fusion inference. *Journal of chemical information and modeling* **61**, 1583–1592 (2021).

[23] Schütt, K. *et al.* Schnet: A continuous-filter convolutional neural network for modeling quantum interactions. *Advances in neural information processing systems* **30** (2017).

[24] Satorras, V. G., Hoogeboom, E. & Welling, M. E (n) equivariant graph neural networks. In *International conference on machine learning*, 9323–9332 (PMLR, 2021).

[25] Yang, Z., Zhong, W., Lv, Q., Dong, T. & Yu-Chian Chen, C. Geometric interaction graph neural network for predicting protein-ligand binding affinities from 3d structures (gign). *The Journal of Physical Chemistry Letters* **14**, 2020–2033 (2023).

[26] Liu, Z. *et al.* Forging the basis for developing protein–ligand interaction scoring functions. *Accounts of chemical research* **50**, 302–309 (2017).

[27] Jumper, J. *et al.* Highly accurate protein structure prediction with alphafold. *Nature* **596**, 583–589 (2021).

[28] Evans, R. *et al.* Protein complex prediction with alphafold-multimer. *biorxiv* 2021–10 (2021).

[29] Lin, Z. *et al.* Evolutionary-scale prediction of atomic-level protein structure with a language model. *Science* **379**, 1123–1130 (2023).

[30] Lin, Z. *et al.* Language models of protein sequences at the scale of evolution enable accurate structure prediction. *BioRxiv* **2022**, 500902 (2022).

[31] Mirdita, M. *et al.* Colabfold: making protein folding accessible to all. *Nature methods* **19**, 679–682 (2022).

[32] Baek, M. *et al.* Accurate prediction of protein structures and interactions using a three-track neural network. *Science* **373**, 871–876 (2021).

[33] Wu, R. *et al.* High-resolution de novo structure prediction from primary sequence. *BioRxiv* 2022–07 (2022).

[34] Krishna, R. *et al.* Generalized biomolecular modeling and design with rosettafold all-atom. *Science* eadl2528 (2024).

[35] Hekkelman, M. L., de Vries, I., Joosten, R. P. & Perrakis, A. Alphafill: enriching alphafold models with ligands and cofactors. *Nature Methods* **20**, 205–213 (2023).

[36] Corso, G., Stärk, H., Jing, B., Barzilay, R. & Jaakkola, T. Diffdock: Diffusion steps, twists, and turns for molecular docking. *arXiv preprint arXiv:2210.01776* (2022).

[37] Stärk, H., Ganea, O., Pattanaik, L., Barzilay, R. & Jaakkola, T. Equibind: Geometric deep learning for drug binding structure prediction. In *International conference on machine learning*, 20503–20521 (PMLR, 2022).

[38] Lu, W. *et al.* Tankbind: Trigonometry-aware neural networks for drug-protein binding structure prediction. *Advances in neural information processing systems* **35**, 7236–7249 (2022).

[39] Zhou, G. *et al.* Uni-mol: A universal 3d molecular representation learning framework (2023).

[40] Davis, M. I. *et al.* Comprehensive analysis of kinase inhibitor selectivity. *Nature Biotechnology* **29**, 1046–1051 (2011).

[41] Steinegger, M. & Söding, J. Mmseqs2 enables sensitive protein sequence searching for the analysis of massive data sets. *Nature biotechnology* **35**, 1026–1028 (2017).

[42] Eastman, P. *et al.* Openmm 4: a reusable, extensible, hardware independent library for high performance molecular simulation. *Journal of chemical theory and computation* **9**, 461–469 (2013).

[43] Kim, S. *et al.* Pubchem 2019 update: improved access to chemical data. *Nucleic acids research* **47**, D1102–D1109 (2019).

[44] Berman, H. M. *et al.* The protein data bank. *Nucleic acids research* **28**, 235–242 (2000).

[45] Cock, P. J. *et al.* Biopython: freely available python tools for computational molecular biology and bioinformatics. *Bioinformatics* **25**, 1422 (2009).

[46] Karelina, M., Noh, J. J. & Dror, R. O. How accurately can one predict drug binding modes using alphafold models? *Elife* **12**, RP89386 (2023).

[47] Corso, G. *et al.* Deep confident steps to new pockets: Strategies for docking generalization. *arXiv preprint arXiv:2402.18396* (2024).

[48] Lu, W. *et al.* Dynamicbind: predicting ligand-specific protein-ligand complex structure with a deep equivariant generative model. *Nature Communications* **15**, 1071 (2024).